The Astrophysical Journal, 693:1666–1677, 2009 March 10 doi:10.1088/0004-637X/693/2/1666

INVESTIGATION OF THICKNESS AND ELECTRICAL RESISTIVITY OF THE CURRENT SHEETS IN SOLAR ERUPTIONS

J. Lin[1,2], J. Li[3], Y.-K. Ko[2], and J. C. Raymond[2]
[1] National Astronomical Observatories of China/Yunnan Astronomical Observatory, Chinese Academy of Sciences, P.O. Box 110, Kunming, Yunnan 650011, China
[2] Harvard-Smithsonian Center for Astrophysics, 60 Garden Street, Cambridge, MA 02138, USA
[3] Institute for Astronomy, University of Hawaii, Honolulu, HI 96822, USA
Received 2007 November 3; accepted 2008 December 8; published 2009 March 10

ABSTRACT

A discussion of the thickness of current sheets in solar eruptions, d, led Lin et al. in 2007 to estimate very large values for the effective resistivity, η_e. Here, we address some questions raised by that paper. We apply the limb synoptic map technique and find d between 5.0×10^4 and 4.6×10^5 km, increasing with both time and altitude. The possibility that large apparent d and η_e result from projection effects is examined and rejected. We derive theoretical scaling laws relating d to other observables that corroborate this conclusion and thus help confine both d and η_e to a reasonable range. The possible impact of our results on the existing models of particle acceleration in reconnecting current sheets is also briefly discussed.

Key words: diffusion – Sun: coronal mass ejections (CMEs) – Sun: flares – Sun: magnetic fields – turbulence

Online-only material: color figures

1. INTRODUCTION

Magnetic reconnection is at the core of many dynamic phenomena in the universe, including solar eruptions, geomagnetic substorms, and tokamak disruptions. Most of the universe is in the form of a plasma threaded by a magnetic field. When twisted or sheared, the field lines may reconnect rapidly, converting magnetic energy into heat and kinetic energy (e.g., Priest & Forbes 2000). Because these phenomena often occur in environments of very high electric conductivity, the process of energy conversion is usually confined to a small local region, such as an X-type neutral point, a current sheet, or a quasi-separatrix layer.

In this work, we focus on the current sheet developed during a solar eruption, connecting a coronal mass ejection (CME) and the associated flare. Generally, a current sheet is a thin current-carrying layer across which the magnetic field changes in either direction or magnitude or both. Definitions and expected interior features of the current sheet may differ among models for the magnetic reconnection process (e.g., see Priest & Forbes 2000). Here, we use the terms "diffusion," "dissipation," and "current sheet" in a more general sense than are used traditionally to refer to any process that causes magnetic diffusion and any region where such diffusion occurs (e.g., see also Lin & Forbes 2000). In this sense, parameters of interest should be considered effective and average. These parameters include the electric resistivity, η_e, of the sheet, and the sheet thickness d determined by either high temperatures observed by Ultraviolet Coronagraph Spectrometer (UVCS) or high densities observed by Large Angle and Spectrometric Coronagraph Experiment (LASCO).

It is traditionally expected that the current sheet is too thin to be observable since its thickness, d, is believed to be roughly the proton Larmor radius, which is about tens of meters in the coronal environment (Litvinenko 1996; Wood & Neukirch 2005, and references therein). This view is based on magnetic reconnection on small scales in the laboratory (with the size of tens of meters) or on quasi-static processes in space (with the timescale of tens of hours or even a few days).

However, CME/flare current sheets form and develop in a highly dynamical fashion during a solar eruption. Theoretical calculations (e.g., Lin & Forbes 2000; Forbes & Lin 2000; Lin 2002) indicate that the current sheet in major eruptive processes could evolve and extend in length at speed up to 10^2 km s^{-1}, and observational results of Ko et al. (2003) and Lin et al. (2005) suggest rapid evolution of the current sheet in major eruptions. In such a highly dynamical process, the scale, especially the thickness, of the current sheet should not be as simple as the Larmor radius of particles. Instead various plasma instabilities must inevitably occur and play an important role in governing the scale of the current sheet (Strauss 1988).

With the improvement in observing techniques during the last decade, more and more direct evidence of magnetic reconnection and current sheets has accumulated, and our knowledge about the related issues has improved (e.g., see Ciaravella et al. 2002; Ko et al. 2003; Webb et al. 2003; Chen et al. 2004; Lin et al. 2005). Recently, Lin et al. (2007) studied two important parameters, the thickness d and effective resistivity η_e, for the CME/flare current sheets in several events.

As a follow-up to Lin et al. (2007), we start by summarizing the results of Lin et al. (2007), and then deducing d for the same events via the approach known as limb synoptic maps (LSMs; Li et al. 2000). In Section 3, we look into the impact of projection effects. The physical causes for broadening the current sheets and observational consequences are studied in Section 4, possible causes of the high effective resistivity of the sheet are discussed in Section 5, and we finally conclude this work in Section 6.

2. OBSERVATIONS AND RESULTS

Several events that developed current sheets between solar flares and the associated CMEs have been studied (Ciaravella et al. 2002; Ko et al. 2003; Webb et al. 2003; Lin et al. 2005, 2007; Bemporad et al. 2006), and in three of them the sheet thickness d and the effective resistivity η_e were investigated (Lin et al. 2007). For each of the three events, Lin et al. (2007)

estimated both the upper and lower limits to d via different approaches. Here, we briefly summarize some important results for the sheets obtained in previous studies, then we utilize the method of the LSMs (Li et al. 2000) to measure the sheet thickness.

2.1. Synopsis of Previous Work

The 1998 March 23 event is the first one used to study the properties of CME/flare sheets (Ciaravella et al. 2002) in the framework of the Lin & Forbes (2000) model. It developed a typical CME–current sheet–flare loop structure, and emission from [Fe XVIII] and other high-temperature lines was identified at the position where the sheet is presumed to be located. The composite of the LASCO C1 image and two UVCS slit images at around 1.5 $R_\odot$ (see Figure 3 of Ciaravella et al. 2002) shows a bright narrow feature appearing in [Fe XVIII] at a polar angle (PA) of 257° and a heliocentric distance of 1.5 $R_\odot$. The current sheet is identified from the [Fe XVIII] intensity distribution along the slit (see also the right-bottom panel in Figure 4 of Ciaravella et al. 2002). The FWHM of the distribution yields an apparent sheet size of about 1.1×10^5 km.

The event of 2002 January 8 is the second event observed by UVCS. The current sheet was long and thin, and it intersected the UVCS slit at right angles. The emission from very hot spectral lines, such as [Fe XVIII], allows us to deduce the sheet thickness d from the distribution of line intensities along the UVCS slit (e.g., see Ko et al. 2003). Figure 1 shows intensity distributions of [Fe XVIII] during two time intervals: 20:46 UT to 23:19 UT on January 10, and 23:21 UT on January 10 to 03:18 UT on January 11. The histograms are the observational data, and the dotted lines are the corresponding Gaussian profiles. The FWHM of the Gaussian in polar angle is $\Delta PA = 7.^\circ 2$. At 1.53 $R_\odot$, this yields an apparent sheet size of 1.3×10^5 km. As a result of projection effects, the above two apparent sizes of the current sheet are upper limits to d.

In the spirit of the work by Ko et al. (2003) and Yokoyama et al. (2001), Lin et al. (2005) investigated a similar event that took place over the east limb on 2003 November 18, and was observed by several instruments both on ground and in space. In this event, the magnetic structures stretched rapidly as the eruption began and the two legs of the stretched structures soon started moving toward one another, approaching the presumed current sheet located between them. The whole process was recorded in both EIT 195 Å movies and UVCS slit images in Lyα (e.g., see Figures 2 and 5 of Lin et al. 2005, respectively). The region where the current sheet was presumed to lie appeared as a dark gap in the Lyα images, which gradually disappeared. The dark gap was interpreted as a current sheet sandwiched between bright regions due to plasma that was continuously swept into the sheet by the reconnection inflow. The narrowing of the gap is unlikely to be just a readjustment of the magnetic field after the overexpansion following the CME, because growing flare loops are observed just below the gap. The process of dimming and recovery in Lyα was used by Lin et al. (2005) to infer the reconnection inflow velocity near the current sheet, and by Lin et al. (2007) to estimate the sheet thickness, yielding an upper limit to d of around 6.8×10^4 km.

2.2. Thickness Deduced from LASCO White-Light Images

The current sheets developed by both the 2002 January 8 event and the 2003 November 18 event were observed roughly edge-on above the limb of the Sun, allowing us to use the

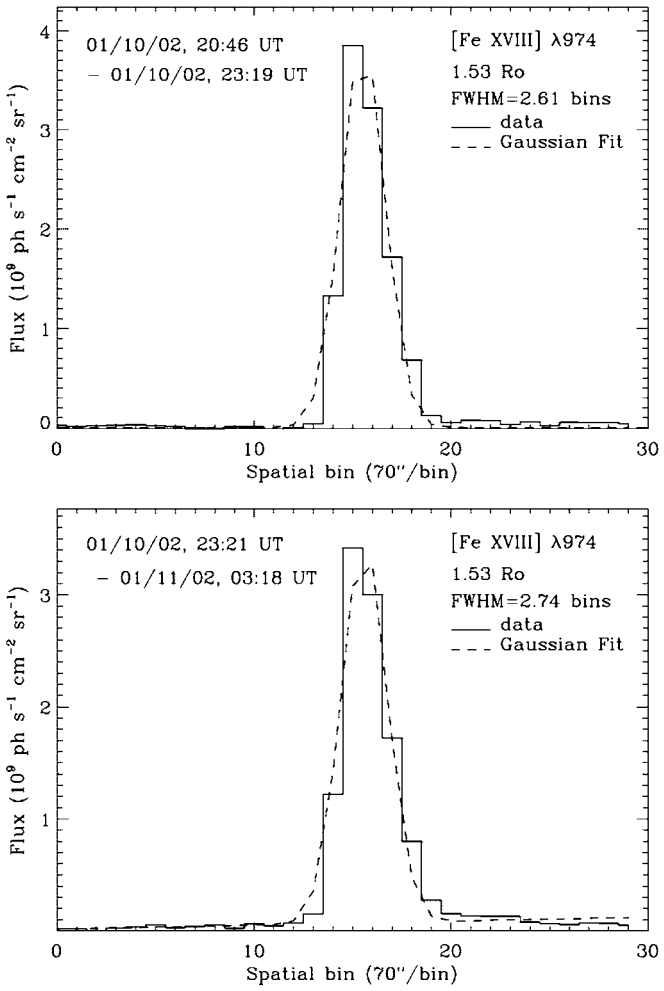

Figure 1. Distributions of the [Fe XVIII] intensity along the UVCS slit in two time intervals. Upper panel: 20:46 UT to 23:19 UT on January 10, and lower panel: 23:21 UT on January 10 to 03:18 UT on January 11. Histograms in both panels are the observational data, and the dotted curves are Gaussian profiles fitted to the data.

LSM technique to estimate d from LASCO white-light images directly. An LSM is made by extracting a narrow strip around the solar limb at a fixed altitude from an image, and then aligning the strips in time sequences (e.g., see Li et al. 2000). It displays the position and/or displacement of an object in PA at various altitudes and times, helps determine the scale (especially d) of some smaller features like the current sheets in a simple and straightforward fashion, and makes it easy to measure d as a function of height.

Figure 2 displays two LSMs of the 2002 January event. These LSMs were constructed by summing over the C2 white-light signals from 3.0 to 3.5 $R_\odot$ (upper panel) and from 5.0 to 5.5 $R_\odot$ (lower panel), respectively, for each time sequence of C2 images. The current sheet in LSM appears as a curved bright feature extending in the horizontal direction (time domain) and moving in the vertical direction (PA domain). The motion of the sheet in the vertical direction was related to the self-adjustment of the magnetic structure after the CME (see also Ko et al. 2003 for more discussion). More LSMs from C2 images covering the altitude interval between 2.2 and 5.5 $R_\odot$, and those from C3 images covering the interval from 4.0 to 9.5 $R_\odot$ are available at this site: http//www.ifa.hawaii.edu/users/jing/CurrentSheet/20020108.html. The time interval covered was from 12:00 UT on January 8 to 00:00 UT on January 12.

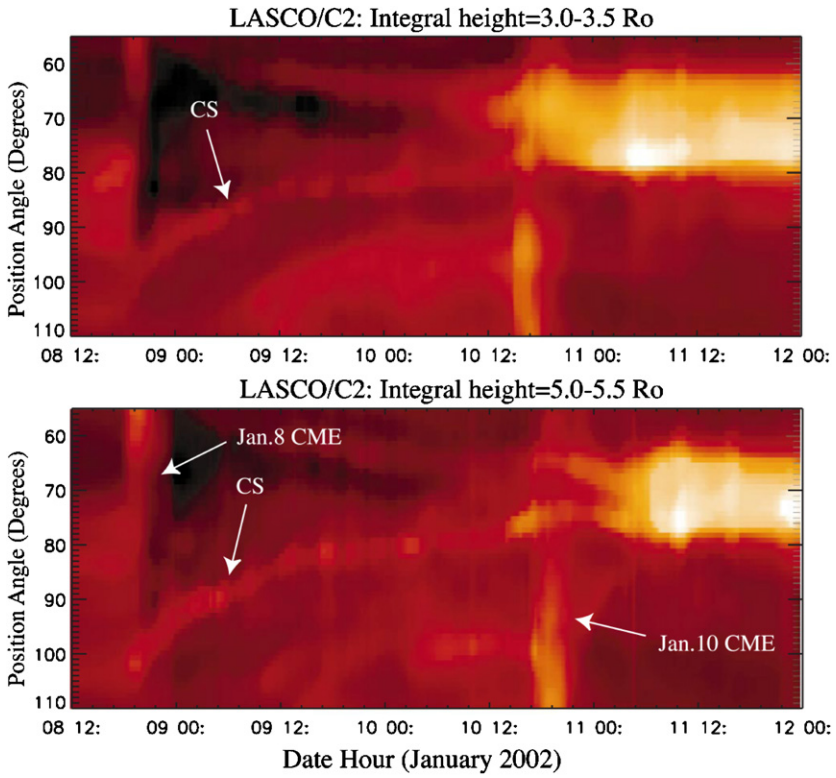

Figure 2. LSMs from LASCO C2 of the 2002 January 8 event covering the altitude interval from 3.0 to 3.5 $R_\odot$ (upper panel) and from 5.0 to 5.5 $R_\odot$ (lower panel), clearly showing the latitudinal movement of the current sheet with time. The current sheet moved about 20° in latitude in the course of 1 day. The 2002 January 10 CME can also be seen to temporarily push the sheet northward (from Ko et al. 2003).

(A color version of this figure is available in the online journal.)

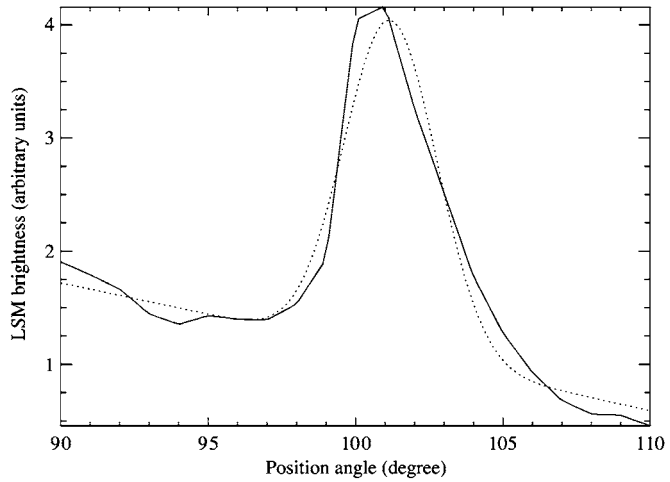

Figure 3. Example of brightness distribution as a function of PA deduced from LSMs. The solid curve is from observations, and the dotted one is the Gaussian profile used to fit the observational data. The FWHM of the Gaussian profile gives the angular measure of d.

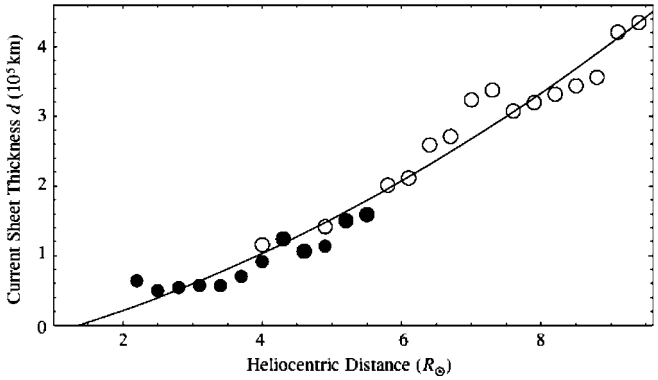

Figure 4. Variations of d against altitude deduced from Figures 2 and 3. The solid circles are from C2 data, and the open ones from C3 data. The solid curve displays the quadratic fitting results. Because of the difference in spatial resolutions between C2 and C3 images as well as in time when C2 and C3 data were taken, some deviation between the values deduced from C2 and C3 images is expected.

From the LSMs we measure the thickness of the current sheet d. Figure 3 displays an example. From the LSM at an altitude R and a given time interval, we obtain the distribution of the brightness (or intensity) versus PA (the solid curve in Figure 3). We use a weighted Gaussian profile (the dotted curve in Figure 3) to fit the brightness distribution, and the FWHM of the profile gives the angular measure of d. The product of this measure with R yields the linear value of d.

Figure 4 plots d derived from Figures 2 and 3 versus height for the time interval from 18:43 UT to 20:09 UT on January 9. It shows that d ranges from 5×10^4 to 4.5×10^5 km between 2.2 and 9.5 $R_\odot$. Comparing these values with those obtained earlier at smaller R by using the high-temperature spectral line profiles, we see that the current sheet expands in both space and time. The expansion in time could result from the magnetic field diffusion via reconnection in the sheet itself, which continues to weaken the surrounding field, and that in space should result from weakening of the magnetic field at high altitudes, where it becomes difficult for the field to confine the sheet.

Panels in Figure 5 display the LSMs for the event of 2003 November 18. As in Figure 2, the current sheet appears as

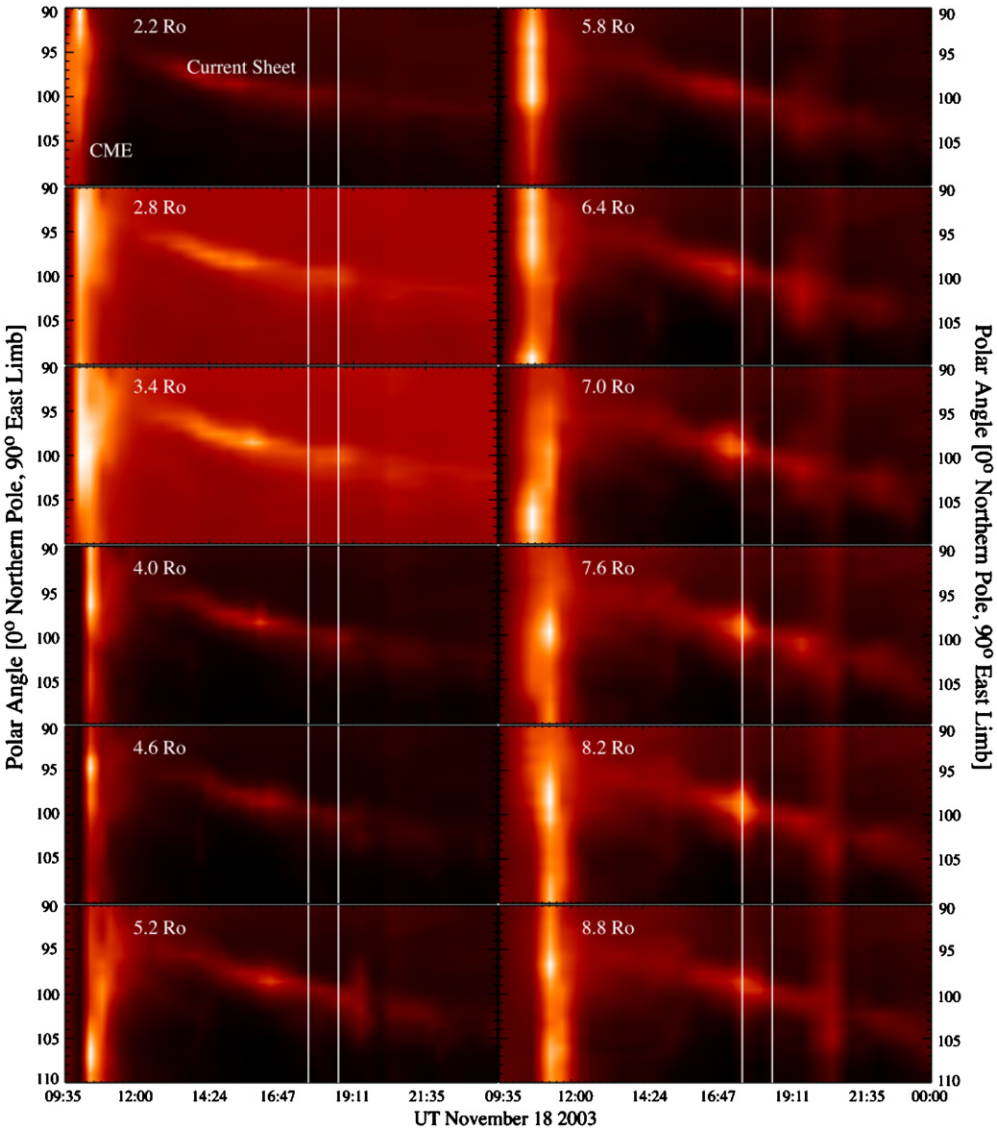

Figure 5. LSM panels for the 2003 November 18 event. The panels in the left column were made from the LASCO C2 data and those in the right column were from C3 data. The two white vertical lines indicate the positions where the data were used to deduce *d*.

(A color version of this figure is available in the online journal.)

a bright feature extending outward in time and moving in PA. These LSMs cover the time interval from 09:35 UT on November 18 to 00:00 UT on November 19. The panels at left were from LASCO C2 data covering *R* between 2.2 and 5.2 $R_\odot$ and those at right from C3 cover 5.8 to 8.8 $R_\odot$.

The current sheet is a bright feature in LSMs from LASCO images, but it is a dark gap in Lyα images (Figure 5; and Figures 5 and 11(a) of Lin et al. 2005). Identifying the dark region in Lyα with the bright ray in white-light seems counterintuitive, but Lin et al. (2005) pointed out that Doppler dimming (Noci et al. 1987) in Lyα images due to a substantial speed of the reconnection outflow along the sheet accounts for the dark gap, and that the relatively high plasma density in the current sheet (see Equation (3.28) of Pudovkin & Semenov 1985) increases the white-light brightness. Furthermore, the white-light brightness depends on the electron density and the Lyα brightness depends on the H I density.

Figure 6 plots the corresponding values of *d* versus *R* deduced from LSMs in Figure 5 via the same approach indicated by Figure 3. As indicated by the two vertical white lines in Figure 5, the data used to deduce *d* were taken in the time interval from 17:42:43 to 18:41:44 UT. As in Figure 4, the plot suggests an increase in *d* from 9.5×10^4 to 7.6×10^5 km from 2.2 and 9.5 $R_\odot$.

We note here that distinct plasma blobs may cause apparent extra broadening of the sheet. The plots in both Figures 4 and 6 purposely avoid the sites where these distinct plasma blobs appear. However, for the event of 2003 November 18, the blobs at altitudes 6.4 through 9.5 $R_\odot$ could not be avoided, which resulted in the deviation of the four points at the right-upper corner in Figure 6 from the d–R curve. If the impact caused by those distinct blobs is partly reduced, the range of *d* shrinks to between 9.5×10^4 and 4.6×10^5 km within the same *R* interval. Eliminating the blobs is problematic in that it is the formation and development of those blobs that broadens the current sheets according to either the tearing mode or the Petschek-type reconnection. For the time being, we avoid the blobs in order to provide an observational lower limit to *d*.

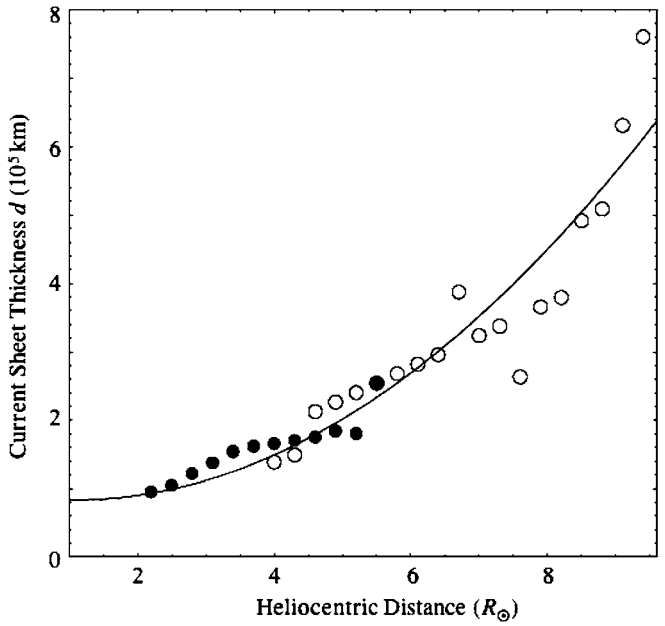

Figure 6. Same as Figure 4, but for the 2003 November 18 event.

3. PROJECTION EFFECTS IN CME/FLARE CURRENT SHEET WIDTHS

Because of projection effects and possible complex morphology of the current sheet and the associated magnetic field, the above values for d are upper limits. As a result of the modest emission measure (EM) of the CME/flare current sheets compared to that of the nearby corona, on the other hand, the current sheet may be faint and difficult to detect if it is not observed roughly edge-on. Below, we investigate how projection effects impact our results for d.

All the images we analyzed above are projections of the emission from an optically thin three-dimensional structure onto the two-dimensional plane of a detector. Since the intensity recorded by the detector is an integration of the total emission along the line of sight (LOS), the intensity level is related to both the density and the column depth along the LOS. Therefore, viewing a bright object at various angles may yield different impressions (see Figure 15 of Forbes & Acton 1996). For a current sheet of given d and extent in other dimensions, seeing it edge-on results largest integral path and thus the largest EM, and seeing it face-on, on the other hand, results in the shortest path and the lowest EM.

Suppose the current sheet is a plate of thickness d and depth D (Figure 7) and the LOS is in the x-direction. In the case of a bright sheet appearing in the dark background, as in the LASCO images, the brightness, b, of the sheet is linearly dependent on the length of LOS inside the sheet. For simplicity, the plasma density in the background is set to be zero. If the current sheet is observed edge-on (see the upper panel in Figure 7) and LOS is parallel to the long axis of the sheet, the observed thickness of the sheet is its natural thickness, d, and its brightness (or the EM) b is proportional to the path along LOS in the sheet $s = D$, $b = \alpha s$, where α is a constant. If the current sheet is tilted by an angle θ, the observed sheet thickness becomes d' and the path along LOS becomes $s = D'$ (see the middle and lower panels in Figure 7).

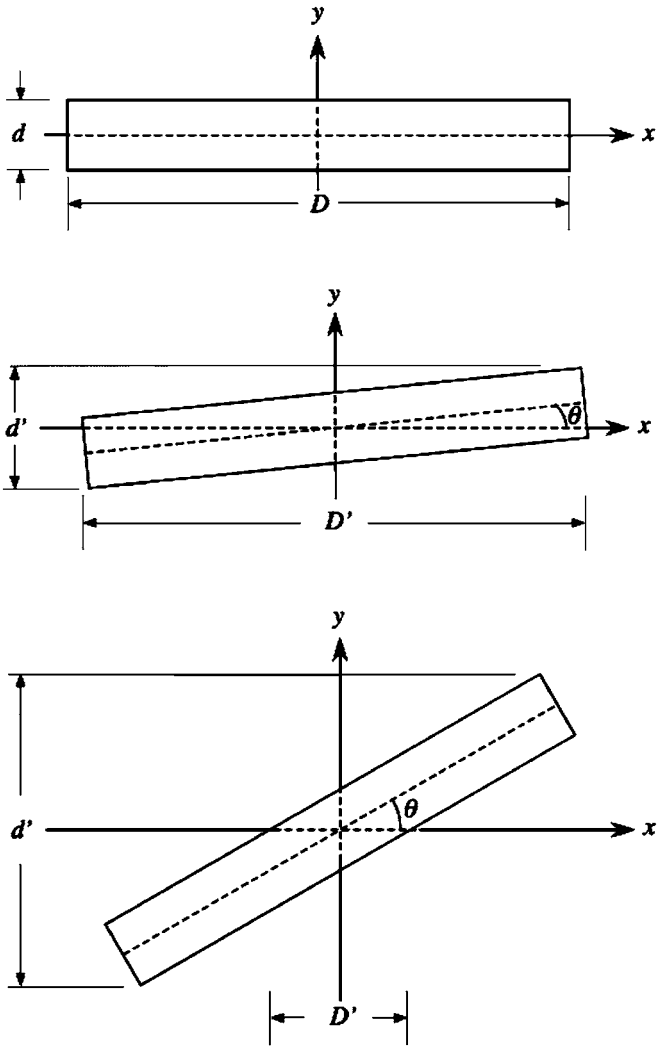

Figure 7. Schematic diagram of orientations of the sheet and the corresponding parameters for the sheet properties. Upper panel: the sheet is observed edge-on; middle panel: the sheet is observed at a small angle; lower panel: the sheet is observed at a large angle.

The orientation of the sheet shown in the middle panel of Figure 7 indicates that for $\tan\theta \leqslant d/D$,

$$s' = D' = D/\cos\theta \quad \text{and} \quad d' = D\sin\theta + d\cos\theta. \tag{1}$$

Usually, $D \gg d$, so $\tan\theta \leqslant d/D$ implies that

$$\frac{s'}{s} \approx 1, \quad \text{and thus} \quad \frac{b'}{b} \approx 1.$$

Furthermore, we have

$$\frac{d'}{d} = \frac{D}{d}\sin\theta + \cos\theta \approx \frac{D}{d}\tan\theta + \cos\theta \leqslant 1 + 1 = 2,$$

considering $\sin\theta \approx \tan\theta \leqslant d/D$ for small θ. Therefore, the observed thickness d' does not exceed two times the natural thickness d and the brightness remains roughly unchanged as θ is small.

If θ is large, say $\tan\theta > d/D$ (see the lower panel in Figure 7), on the other hand, we have

$$d' = D\sin\theta + d\cos\theta,\ s' = D' = d/\sin\theta \quad \text{and}$$
$$\frac{b'}{b} = \frac{D'}{D} = \frac{d}{D\sin\theta}. \tag{2}$$

From the first equation in Equation (2),

$$\frac{D\sin\theta}{d} = \frac{d'}{d} - \cos\theta, \tag{3}$$

and therefore

$$\frac{b'}{b} = \frac{1}{d'/d - \cos\theta}. \tag{4}$$

Therefore, the brightness of the sheet is roughly inversely proportional to the observed thickness of the sheet. This implies only a limited impact of projection effects on measuring d.

Equations (1) and (2) indicate that the sheet thickness can be obtained directly from observations in two cases: $d = d'$ for $\theta = 0°$, and $d = D'$ for $\theta = 90°$. Generally, d' is measured from the sheet images in a straightforward fashion, and D' is deduced through spectroscopic approaches. In practice, the EM determined from a collisionally excited spectral line, EM, is proportional to $n_e^2 D'$, and the brightness of the scattered Lyα line, $I_{\mathrm{Ly}\alpha}$, is proportional to $n_e D'$. Therefore, with EM and $I_{\mathrm{Ly}\alpha}$ being deduced from observations, we have $n_e \sim \mathrm{EM}/I_{\mathrm{Ly}\alpha}$ and $D' \sim I_{\mathrm{Ly}\alpha}^2/\mathrm{EM}$. Furthermore, comparison of d' with D' reveals whether projection effects are important or not: if d' is small compared to D', projection effects are trivial in measuring the sheet thickness d according to Equation (1); if they are comparable to each other, Equation (2) suggests that a serious consideration of projection effects is necessary. For the 2003 November 4 event, Ciaravella & Raymond (2008) used the polarized brightness, pB, from Mauna Loa Solar Observatory (MLSO) coronagraphs to get the electron column density, $N_e = n_e s$, and the EM from [Fe XVIII], $n_e^2 s$ to determine n_e and s. They found $d'/d = 4$.

In the case of the dark gap surrounded by the bright features observed in Lyα (see Figures 5 and 11(a) of Lin et al. 2005), the brightness of the sheet is replaced by the contrast of the gap to the surrounding features. A gap like that in Lyα emission can also be artificially broadened by projection of a thin sheet not quite parallel to LOS. As with the brightness, however, any such broadening would cause a corresponding reduction in contrast. The reduction in the contrast is roughly inversely proportional to broadening of the gap. Therefore, a completely dark current sheet in Lyα emission that appears 10 times wider than its natural thickness will have only 10% contrast.

This result justifies the conclusion of Lin et al. (2007) that the value of d deduced from the Lyα gap for 2003 November 18 event should not differ much from the true value of d although it is still considered as the upper limit. The Lyα gap in the event was 2–4 times fainter than the adjacent Lyα emission (see Figure 11(a) of Lin et al. 2005), which implies the contrast of 0.5–0.75. Because these values do not greatly differ from the unity, we then conclude that projection effects in this event do not increase the apparent thickness by more than a factor of 2–3.

4. CURRENT SHEET BROADENING AND OBSERVATIONAL CONSEQUENCES

The CME/flare current sheet thicknesses we obtain are very different from those expected on the basis of the *Spitzer* or the anomalous resistivity (e.g., see Priest 1982; Litvinenko 1996; Wood & Neukirch 2005). Our previous discussion indicates that projection effects cannot account for the observed broadened current sheets, and the recent work of Bemporad et al. (2006) implies that the impact of complex morphology is limited. We thus need to consider physical mechanisms for large thicknesses of CME/flare current sheets.

Here, we address reasons for these thicknesses in the context of existing reconnection theories, and two versions of reconnection are discussed: turbulent reconnection due to the tearing mode instability and time-dependent Petschek-type reconnection. These are only two of many possible processes that could broaden the sheet and produce other observational features of the sheet, but given the current limited knowledge of detailed processes inside the CME/flare current sheets, we confine ourselves to these two mechanisms for the time being.

4.1. The Current Sheet Undergoing Tearing

The tearing mode instability is a long-wavelength resistive instability first investigated by Furth et al. (1963) in the framework of resistive instability modes established by Dungey (1958). At an X-type neutral point, finite conductivity can give rise to an unstably growing current concentration, and a current sheet can tear along current-flow lines, forming a chain of filaments, or magnetic islands in projection (Figure 8). We take k to be the wave number of the turbulence caused by the instability and $l = d/2$ to be the half thickness of the sheet.

The growth time scale τ of the modes must be longer than τ_A, but shorter than τ_d:

$$\tau_A < \tau < \tau_d, \tag{5}$$

where $\tau_A = l/V_A$ and $\tau_d = l^2/\eta$ are the times in which an Alfvén wave and resistive diffusion traverse the sheet, respectively. Here, V_A is the local Alfvén speed near the current sheet and η is the magnetic diffusivity of the sheet.

In the case of the tearing mode in a simple sheet structure investigated by Furth et al. (1963) with the "constant-ψ" approximation (namely fluctuations in B_y are small), inequalities in Equation (5) imply that

$$S^{-1/4} < \bar{k} < 1, \tag{6}$$

where $\bar{k} = kl$, and $S = \tau_d/\tau_A$ is the Lundquist number of the current sheet (see Priest & Forbes 2000, p. 180).

For different initial and internal magnetic structures inside the current sheet, on the other hand, relations of $\bar{k}$ to S may differ from those shown in Equation (6). For example, Bobrova & Syrovatskii (1980) derived analytic solutions for the growth rate of the instability in a current sheet with a periodic internal structure. They obtained

$$S^{-1/7} < \bar{k} < 1, \tag{7}$$

which implies a larger lower limit of $\bar{k}$ compared to that determined by Equation (6).

However, the "constant-ψ" approximation breaks down for the double or multiple tearing mode, and very large values of S and $\bar{k}^{-1}$ (e.g., see Priest 1985). Stix (1976) and Rechester & Stix (1976) found that, when the current sheet in equilibrium includes two or more layers (Figure 9; see also Figures 1 and 2 of Drake et al. 2006) that are close together, the linear growth rate of the tearing is greatly enhanced. Full particle simulations performed by Drake et al. (2006) showed that the interior features in the sheet as shown in Figure 9 may develop from

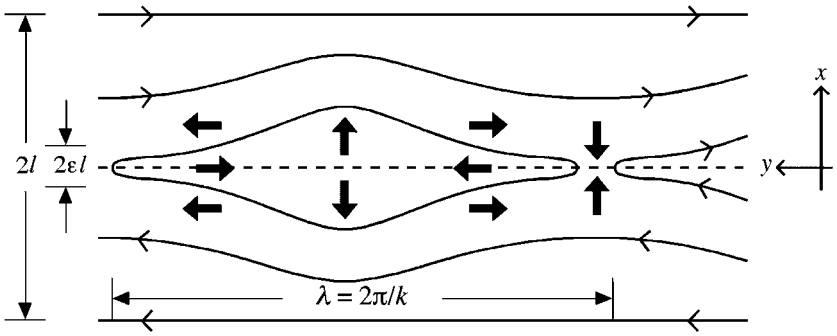

Figure 8. Interior structure of the current sheet in which the tearing mode instability develops. The thick arrows show plasma flow and the thin arrows are for magnetic field lines (courtesy of E. R. Priest).

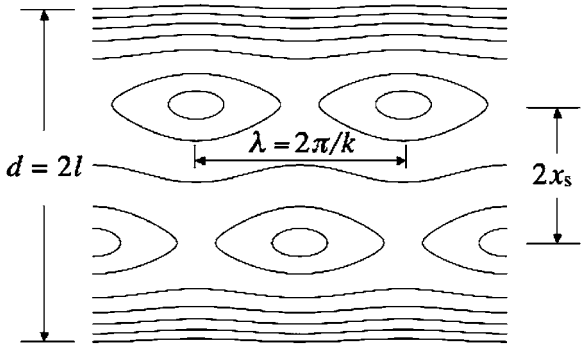

Figure 9. Interior structure of the current sheet undergoing the double tearing mode instability with x_s being the half separation of the two layers, and other notes the same as those in Figure 8.

a large-scale X-type neutral point when a guide field exists. Since the simulations have a limited spatial extent, on the other hand, Drake et al. (2006) could not give any scale similar to those shown in Equations (6) and (7).

Pritchett et al. (1980) found that the "constant-ψ" approximation is still valid for large enough separation between layers, and the instability develops at the standard tearing growth rate. As the separation becomes small, the "constant-ψ" approximation breaks down, and the dispersion relation for the growth rate leads to (see also Priest 1985)

$$\frac{\tau_A}{\tau} = \left(\frac{\bar{k}^2}{S}\right)^{1/3}, \tag{8}$$

to within a constant depending on the initial configuration. Applying Equation (5) to Equation (8) gives

$$S^{-1} < \bar{k} < S^{1/2}. \tag{9}$$

Recently, Loureiro et al. (2007) looked into the detailed evolutionary features inside a current sheet on which magnetic reconnection inflows were imposed at both sides. The inflow enhances the instability growth rate compared with that of Bulanov et al. (1978). The maximum growth rate scales as $S^{-1/2}$, and the corresponding $\bar{k}$ scales as $S^{-1/4}$. Relations shown in Equations (6), (7), and (9) indicate that $\bar{k}$ could possess a finite lower limit provided that S is not extremely large. This result has an important consequence for helping eliminate projection effects in the results for d deduced directly from the observational data. We can estimate $l_{\rm min}$ or $d_{\rm min}$ via $\bar{k}_{\rm min}$ governed by these relations. Here, $l_{\rm min}$, $d_{\rm min}$, and $\bar{k}_{\rm min}$ are the lower limits to l, d, and $\bar{k}$, respectively.

Following Lin et al. (2007), we first relate $\bar{k}_{\rm min}$ to S and/or M_A. Here, M_A is the Alfvén Mach number of reconnection, which measures the relative rate of reconnection in terms of the inflow speed v_i near the current sheet compared to the local Alfvén speed V_A at the same location (see discussions of M_A by Lin & Forbes 2000). Usually, V_A is not observable, but it is identical with the reconnection outflow speed $v_{\rm out}$ according to the standard theory of magnetic reconnection (see Priest & Forbes 2000, pp. 121–123), so $M_A = v_i/v_{\rm out}$. A series of recent works have shown that both v_i and $v_{\rm out}$ can be obtained via direct observations of the CME/flare current sheet (Ko et al. 2003; Lin et al. 2005; Riley et al. 2007). In the work of Yokoyama et al. (2001), on the other hand, $v_{\rm out}$ was not deduced directly from observations. Instead they made two reasonable efforts to guess the magnetic field around the reconnection, estimated V_A with the plasma density being deduced independently, and then obtained the rate of reconnection through $M_A = v_i/V_A$.

According to Lin et al. (2007), S is related to M_A by

$$S = v_{\rm out}/v_i = M_A^{-1}. \tag{10}$$

We are now able to relate $l_{\rm min}$ to M_A with Equation (10) for different cases such that

$$l_{\rm min} = M_A^{1/4}\frac{\lambda}{2\pi}, \tag{11}$$

$$l_{\rm min} = M_A^{1/7}\frac{\lambda}{2\pi}, \tag{12}$$

$$l_{\rm min} = M_A\frac{\lambda}{2\pi}, \tag{13}$$

from Equations (6), (7), and (8), respectively. Here, $\lambda = 2\pi/k$ as specified in Figures (8) or (9). Equations (11), (12), and (13) indicate that a current sheet that undergoes the tearing mode should have a minimum thickness that depends on the rate of magnetic reconnection and the distance between magnetic islands. Different scales of M_A displayed by Equations (11), (12), and (13) imply the role of the sheet initial and internal properties in governing its thickness, and Equation (13) gives the smallest value of $l_{\rm min}$ as a result of the fact that $M_A < 1$. It is interesting to note that Strauss (1988) obtained the same scaling as Equation (13) via a different approach based on the argument that the reconnection outflow can suppress the tearing modes by convecting them away unless they grow faster than they are convected away. The observational consequence of these equations is that $l_{\rm min}$ can be estimated if M_A and λ

can be determined. This is an independent way to estimate the thickness, and it can be compared with the direct measurements of d in the previous section.

The thick current sheet could in reality be composed of a large number of small-scale sheets. A recent work by Bemporad (2008) indicates that the size of these small sheets varies from 10 to 10^4 m and there could be up to a few 10^4 such small sheets present in the large-scale sheet in a major eruption. The double tearing mode is a first, though limited, exploration of effects of having many small regions simultaneously reconnecting. Equations (11), (12), and (13) are developed to show the large range of theoretical predictions, and we discuss them as an indication of the uncertainty involved.

For the events studied so far, M_A ranges from 10^{-3} to 10^{-1} (e.g., Yokoyama et al. 2001; Ko et al. 2003; Lin et al. 2005). So S varies from 10 to 10^3, which is small compared to the values of S ($\sim 10^8$–10^{12}) for the quiet corona (e.g., see Priest 1982). The values of S of interest are also within the same range for the sheets occurring in laboratory (Furth et al. 1963; Priest & Forbes 2000).

For the event studied by Lin et al. (2005), both v_i and $v_{\rm out}$ were deduced directly from observational data, and M_A was found to range from 7.8×10^{-3} to 0.18. From Figure 3(d) of Lin et al. (2005), two successive blobs can be recognized simultaneously, and the distance between them is around 5.37 $R_\odot$. Taking this distance as λ in Equation (13) implies $l_{\rm min} = 4.55 \times 10^3$ km. For the event studied by Ko et al. (2003), $v_{\rm out}$ was obtained directly from the motions of the plasma blobs along the sheet, but v_i was approximately estimated according to the motions of the magnetic features near the current sheet. Ko et al. (2003) found M_A between 0.015 and 0.03. The smallest value of λ is 3.1×10^5 km, so $l_{\rm min} = 740$ km.

We note here that the above values of $l_{\rm min}$ were deduced according to Equation (13), which gives the smallest value of $l_{\rm min}$ for the three cases of the tearing mode related to Equations (11) through (13). They are small compared to the observed widths obtained earlier, but estimates from Equations (11) or (12) are just a few times smaller than the observed d. However, the significance of this part of work is not to find the true value of l or d itself, but to study how small $l_{\rm min}$ could be or how thin a CME/flare current sheet in reality could be, and to help eliminate projection effects from the measured values of d. Furthermore, the smallest value of $l_{\rm min}$ we found here is around 10^3 km, which is significantly larger than the values of a few meters suggested by many authors (e.g., see Litvinenko 1996; Wood & Neukirch 2005, and references therein). Thus, the theoretical estimates confirm that the current sheet developed in the CME/flare process could be fairly thick, and even the small value of $l_{\rm min}$ is an interesting constraint on theory.

4.2. Time-Dependent Petschek-Type Reconnection

The most popular picture of reconnection in solar flares is Petschek (1964) reconnection. Since the exhaust region has an opening angle of around 8° (e.g., see Forbes & Malherbe 1991; Vršnak & Skender 2005), this picture could account for thick observed current sheet thickness provided that the thin diffusion region is sufficiently far from the height where the thickness is observed.

The Petschek mechanism does account for most aspects of solar flares. However, most of the dissipation of magnetic energy occurs in slow mode shocks along the edges of the exhaust, which covert the magnetic energy primarily into heating and kinetic energy of the reconnected plasma. To produce enough energetic electrons to account for type III radio bursts and hard X-ray emissions seen in solar flares (e.g., see Miller et al. 1997), one needs to accelerate these electrons in a large enough space filled with plasma turbulence (Tajima & Shibata 2002). The diffusion region in the Petschek-type framework is too small to provide enough electrons, and it may be too small for efficient acceleration as well. In addition, the high temperature implied by [Fe XVIII] emission is the primary signature of a current sheet in UVCS data, which implies strong electron heating. If electrons and protons are heated equally, the [Fe XVIII] emission can be understood. However, Petschek-type reconnection exhausts detected in the solar wind show no sign of electron heating (e.g. Gosling 2007). It is possible that the different values of plasma β in flares from that in the solar wind give more efficient electron heating in CME/flare current sheets. A third difficulty is that Petschek reconnection reverts to much slower Sweet–Parker reconnection if the resistivity is constant (Biskamp 1986, 1990).

In spite of these questions, we wish to compare our observations with both viable reconnection theories, the turbulent and the Petschek pictures. Therefore, we develop the picture of unsteady Petschek reconnection in order to find the relationship between the spacing of ejected blobs of plasma and the current sheet thickness.

Figure 10 displays the process of unsteady Petschek-type reconnection. Petschek (1964) developed a model for the steady-state process, and Semenov et al. (1983a, 1983b, 1984), Pudovkin & Semenov (1985), and Biernat et al. (1987) extended Petschek's original steady-state model to the time-dependent version (see also Priest & Forbes 2000 for a comprehensive review).

In this version, reconnection starts with the diffusion in a localized region (marked by the asterisk signs in Figure 10 for $t = 0$), launching disturbances into the medium at large. Here, the time t is in units of τ_A, and the diffusion is parameterized $M_A(t)$, which also governs the evolution of the hydromagnetic configuration. Figure 10(a) shows an example where a single pulse reconnection occurs (e.g., see also Rijnbeek et al. 1989). The disturbance propagates at the local Alfvén speed at the diffusion region, and a slow mode shock forms in front of the propagating disturbance ($t = 0.5$). Collectively, these slow mode shocks establish an outflow region for plasma and magnetic field streaming toward the current sheet ($t = 1.0$). With the rate of reconnection dropping to zero ($t \geqslant 1.0$), the reconnection inflow stops, but the outflow regions keep expanding.

Biernat et al. (1987) showed that the evolution of both the slow shocks and the outflow regions is determined by the temporal behavior of $M_A(t)$. Here, we apply their results to a disturbance in response to

$$M_A(t) = \frac{1}{20}[1 - \cos(2\pi t)], \tag{14}$$

which describes a bursty-type reconnection. Figures 11 plots the functional behavior of M_A. Panels in Figure 10(b) show a set of snapshots of hydromagnetic configurations in the medium in response to this M_A. Similar blob features are produced in the first period ($t \leqslant 1.0$), and subsequent blobs are produced after $t = 1.0$ and propagate outward.

Another important consequence of $M_A(t)$ given in Equation (14) is broadening of the sheet as a result of formation of the reconnection outflow region surrounded by slow shocks. From Biernat et al. (1987), the location/shape of the

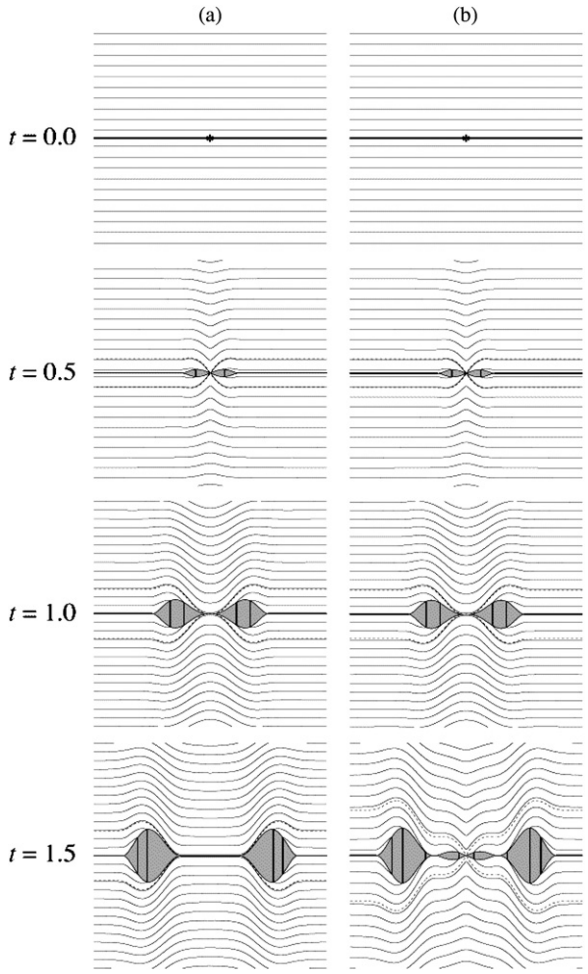

Figure 10. Evolution of the hydromagnetic configuration in time-dependent Petschek-type reconnection in response to single pulse dissipation (*a*), from Rijnbeek et al. (1989), and bursty dissipation (*b*). Panels are snapshots of the hydromagnetic configurations at different times. The asterisks in the panels for $t = 0$ indicate the location where reconnection is initiated, the solid curves describe magnetic field lines, the thick solid lines are for the current sheets, the dashed curves show the separatrices, and the shadowed areas are the reconnection outflow regions surrounded by the slow mode shocks. The *x*-axis points to the right, the *y*-axis points upward, and the origin is colocated with the asterisk. The scale in the *y*-direction in each panel has been enlarged by a factor of 10 in order to show detailed structure of the disturbance.

shock transition that separates the outflow from the inflow is determined by

$$y = -\frac{x}{r_n} M_A(t - x/V_A), \tag{15}$$

where x and y are displacements parallel and perpendicular to the sheet, respectively (see Figure 10), r_n is the plasma density in the outflow region compared to that in the inflow region, and $M_A(t - x/V_A) = 0$ for $t < x/V_A$. This relation gives the thickness of the current sheet broadened by the slow shocks. Averaging each parameter in Equation (15) over the spacetime interval of the shock, we find

$$\bar{l} \approx r_n^{-1} \bar{M}_A \bar{\lambda}, \tag{16}$$

where $\bar{\lambda}$ is the average extent of the shock along the sheet.

Comparing Equation (16) with Equations (11) through (13), which are determined via different approaches, indicates that a similar scaling law relates l to λ. In the low β coronal plasma, we

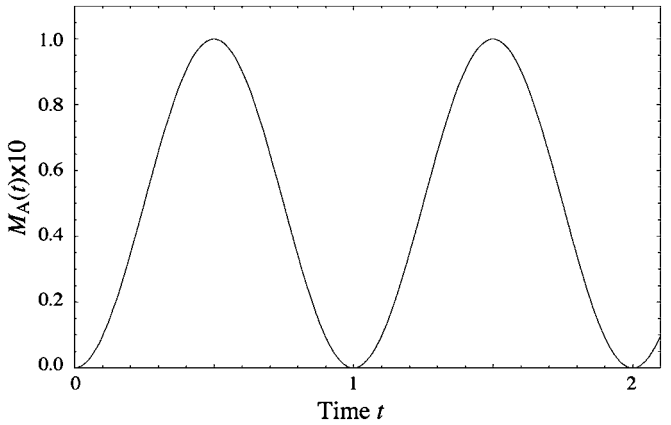

Figure 11. Variations of $M_A(t)$ vs. time as magnetic reconnection bursty as described by (14).

roughly have $r_n = 2.5$ (Equation (3.28) of Pudovkin & Semenov 1985). Therefore, we can estimate the average sheet thickness $\bar{l}$ in the framework of Petschek-type reconnection by assuming that the observed blobs result from bursty reconnection and that $\bar{\lambda}$ is roughly equal to the separation between blobs. For the 2002 January 8 event (Ko et al. 2003; Lin et al. 2007), we have $\bar{\lambda} = 3.1 \times 10^5$ km and $\bar{M}_A = 0.015$, which yields $\bar{l} = 1.86 \times 10^3$ km; and for the 2003 November 18 event (Lin et al. 2005, 2007), we have $\bar{\lambda} = 3.74 \times 10^6$ km and $\bar{M}_A = 7.8 \times 10^{-3}$, which gives $\bar{l} = 1.17 \times 10^4$ km.

Comparison of values of $\bar{l}$ with those of $l_{\min}$ shows that they are the same within a factor between 2 and 3. This implies that the small value of $l_{\min}$ is not very unexpected. Equations (13) and (16) were deduced through different approaches, in which different aspects of magnetic reconnection are addressed, but their equivalence is apparent. The fact that magnetic reconnection is caused by plasma instabilities in the sheet might account for the equivalence of the two approaches. Furthermore, as we mentioned earlier, the importance of these values lies in their implication that the CME/flare current sheet could be much thicker than suggested by many authors (e.g., see Litvinenko 1996; Wood & Neukirch 2005, and references therein). However, the physical picture of a thick current sheet is very different from that of a Petschek-type exhaust flow.

4.3. Reasonable Values of the Current Sheet Thickness and the Corresponding Electrical Resistivity

Because of our limited knowledge of the interior structures of a CME/flare current sheet, we discussed several cases of current sheet broadening, and the corresponding scaling laws relating the sheet thickness to observables. These relations indicate the important role of the small-scale structures inside the current sheet in the energy conversion process. The existence of these structures allows magnetic reconnection in a thick sheet to take place fast enough to support major energy release processes in CMEs and flares, and it yields the linear dependence of the sheet thickness d on the extent λ of these structures along the sheet. Furthermore, the tearing mode turbulence not only broadens the sheet, but also sets up a range for kl, which allows us to evaluate the lower limit of either k or l with either of them being known or fixed. This provides corroboration for the estimate of d.

With known l and v_i, we are able to estimate the corresponding effective electric resistivity, η_e, in the sheet for the cases we studied here. These three parameters are related to one another

such that (e.g., see Priest & Forbes 2000, p. 120)

$$v_i = \frac{\eta}{l}, \qquad \text{with} \quad \eta = \frac{\eta_e}{\mu_0}, \tag{17}$$

where l is in units of m, v_i in m s^{-1}, η is the magnetic diffusivity, $\mu_0 = 4\pi \times 10^{-7}$ H m^{-1} is the permeability of free space. To avoid projection effects, we do not use those values of $d = 2l$ obtained in Section 2 to deduce η_e. Instead we use those deduced from Equation (13) or (16) to determine a lower limit to η_e, and whether turbulence contributes to the resistivity significantly.

For the 2002 January 8 event, with $M_A = 0.015$, $v_i = 10$ km s^{-1}, and $l = 740$ km s^{-1}, we obtain $\eta_e = 9.30 \times 10^3$ ohms m; and for the 2003 November 18 event, with $M_A = 7.8 \times 10^{-3}$, $v_i = 8.42$ km s^{-1}, and $l = 4.55 \times 10^3$ km, we find $\eta_e = 4.81 \times 10^4$ ohms m. Compared with Lin et al. (2007), we use smaller values of $l_{\rm min}$ in order to further eliminate possible projection effects in the observed values of d or l.

As in Lin et al. (2007), the values of η_e obtained here are much larger than the classical and anomalous resistivities. Thus, the role of conventional anomalous resistivity in the reconnecting current sheet is quite limited, and instead the structure of magnetic islands (Ambrosiano et al. 1988; Drake et al. 2006) or slow mode shocks (Petschek 1964) dominates. In the case of a turbulent current sheet, the large η_e is an effective resistivity in the usual sense, while in the Petschek case it is dimensionally the same but does not correspond to electrical resistivity of the plasma.

5. PROCESSES RESPONSIBLE FOR HIGH RESISTIVITIES

Values of d and η_e inferred above for several individual events are much larger than expected. As we mentioned previously, they are in fact averaged quantities over many small-scale processes that determine the sheet properties, and suggest a very efficient diffusion process occurring in the CME/flare sheets. This unusual result is quite probably due to using Equation (17) to relate η to other parameters for the current sheet, which may be valid only for the diffusion caused by the classical or conventional anomalous resistivities, although it might be justified in the effective and average sense. However, theories of plasma turbulence indicate that the turbulence can broaden a current sheet (Strauss 1988; Drake et al. 2006), cause a much higher resistivity, known as hyper-resistivity H (Strauss 1988; Bhattacharjee & Yuan 1995), and perhaps even play an important role in coronal heating (van Ballegooijen & Cranmer 2008).

Hyper-resistivity results from the competition between the amplification and the diffusion of the magnetic field by the tearing turbulence (Bhattacharjee & Yuan 1995). The tearing turbulence starts with diffusing the large-scale magnetic field, then converts part of the magnetic energy into turbulent kinetic energy, which in turn creates perturbed small-scale magnetic fields via the dynamo process. The growth of the perturbed field is controlled by the tearing since the turbulence diffuses the perturbed field created by the tearing modes as well (see Strauss 1986, 1988). This causes more efficient diffusion in the reconnecting current sheet. Small-scale field stochasticity (braiding) produced in this process gives rise to an effective perpendicular momentum transport, hence to an anomalous electron viscosity (see also discussions of Biskamp 1993, p. 22).

Strauss (1988) found that

$$v_i = \frac{H}{l^3},$$

if the dissipation caused by the hyper-resistivity in the current sheet is considered, where H is in unit of m^{4}s^{-1}.

Corresponding to η_e given in Equation (17), we define $D_e = \mu_0 H$. The efficiency of the diffusion caused by D_e and by η_e was compared by Strauss (1988),

$$\frac{D_e}{\eta_e l^2} \approx 0.15 M_A^3 \beta^{1/2} \frac{\omega_{pe}}{ck}, \tag{18}$$

where β is the plasma beta in the current sheet, ω_{pe} is the plasma frequency, and c is the speed of light. For the quiet corona, Strauss (1988) found that the ratio is around 10^9; and for the CME/flare current sheets that were studied in this work, this ratio is at least 10^6 if $\beta = 1$ and $M_A = 10^{-2}$.

Lazarian & Vishniac (1999) studied the role of the stochastic features in the current sheet through a different approach. In this version, magnetic field dissipation starts with Ohmic diffusion, and stochastic components of the magnetic field are produced in the initial stage. The stochastic components cause small-scale "wandering" in the field lines. This allows magnetic reconnection to take place among adjacent wandering field lines (see Figure 2 of Lazarian & Vishniac 1999), yielding multiple reconnection sites within the sheet. The presence of multiple reconnection sites results in a minimum rate of reconnection, $M_A = R_L^{-3/16}$, where R_L is the magnetic Reynolds number in the whole system involved in the energy conversion. In the solar coronal R_L ranges from 10^8 to 10^{12}, which brings the minimum of M_A to 5.6×10^{-3} that is within the range of the observed values. The scaling laws of Lazarian & Vishniac (1999) suggest current sheet thicknesses perhaps an order of magnitude smaller than observed, but much closer to the observed values than the classical values.

Petschek reconnection starts similarly with Ohmic diffusion, but the consequence is a slow mode shock, not a stochastic magnetic field. In this process, the slow mode shock is the crucial agent for the energy conversion, and works equivalently to those small-scale turbulent eddies or stochastic structures inside the sheet. Similar observational consequences, together with our above investigations, suggest the equivalence of different approaches to studying the current sheet and magnetic reconnection. Analogies between the discussions by Forbes & Malherbe (1991) with that by Priest & Forbes (2000, pp. 391–393) of plasma blobs appearing in reconnecting current sheets may further strengthen the impression of such equivalence, but the two pictures have different implications for models of particle acceleration.

6. CONCLUSIONS

We briefly reviewed the results of Lin et al. (2007), and discussed and addressed some issues that were not addressed there. These issues include measuring d by using the LSM techniques, the impact of projection effects on the measurement of d, detailed properties of the mechanisms for broadening the current sheet and for creating plasma blobs observed to flow inside the sheet, and possible applications of these properties to estimate d, as well as the equivalence of observational consequences of different mechanisms.

The main results are summarized as follows.

1. Applying the LSM techniques to the events of 2002 January 8 and 2003 November 18, we inferred d as a follow-up of Lin et al. (2007). Variations of d versus both time and altitude suggest the expansion of the sheet in thickness as a result of the decreasing magnetic field. In the height interval between 2.2 and 9.5 $R_\odot$, d increased from 0.5×10^5 to 4.5×10^5 km in the first event, and from 10^5 to 7.5×10^5 km in the second one. Recent work by Ciaravella & Raymond (2008) for the 2003 November 4 event also finds that d is around 4×10^4 km.
2. In the case of a current sheet seen roughly edge-on, projection effects may broaden the sheet by a factor of 2, but the low density in the sheet causes the sheet to quickly become faint and diffuse as the tilt becomes large. Therefore, the apparent thickness of the reconnecting current sheets is not much greater than the true thickness.
3. Turbulence caused by plasma instabilities and by time-dependent Petschek-type reconnection was investigated as two possible mechanisms for broadening reconnecting sheet. Both mechanisms work well for explaining observations. Although consequences of the two mechanisms are not distinguishable via the present techniques for observing the Sun, and it is very likely that both mechanisms take effect simultaneously, further improvements in both theoretical knowledge and observing techniques will help to solve the problem.
4. The above investigations yielded several scaling laws that relate the current sheet thickness d to other observables that are not sensitive to projection effects. This provides us an approach to estimating the lower limits, $d_{\rm min}$, to d on the basis of the known theoretical results, and thus to constraining the impact of projection effects on the measured values of d. On the other hand, the values of $d_{\rm min}$ obtained from the tearing mode vary from case to case, and some of them show large discrepancies with d measured from observations. Although projection effects may partly account for the discrepancy, the existence of a range of theoretical predictions indicates the uncertainties involved in the existing studies of this problem, and continuing investigations on it are hence necessary.
5. Results of this work should also benefit the study of particle acceleration in CME/flare sheets in two ways: first, in most models for particle acceleration inside the sheet (e.g., see Litvinenko 1996; Wood & Neukirch 2005, and references therein), d is only tens of meters. Our results that the thick current sheet exists may make it easier to confine the particles long enough for acceleration to high energies. Second, various turbulence modes fill the sheet and their interactions with particles could be crucial for determining particle spectra (e.g., see Onofri et al. 2006).

We gratefully acknowledge T. G. Forbes, A. A. van Ballegooijen, G. Poletto, and A. Bemporad for valuable discussions, comments, and suggestions. We also thank the referee for carefully reading the paper, and for providing very helpful and instructive comments and suggestions for improving this paper. J.L., Y.-K.K., and J.C.R. thank ISSI (International Space Science Institute, Bern) for the hospitality provided to the members of the team on the Role of Current Sheets in Solar Eruptive Events where many of the ideas presented in this work have been discussed. J.L.'s work at YNAO was supported by the Ministry of Science and Technology of China under the 973 Program grant 2006CB806303, by the National Natural Science Foundation of China under grants 10873030 and 40636031, and by the Chinese Academy of Sciences under the grant KJCX2-YW-T04 to YNAO; and his work was supported by NASA grant NNX07AL72G when he visited to CfA. *SOHO* is a joint mission of the European Space Agency and the US National Aeronautics and Space Administration.

REFERENCES

Ambrosiano, J., Matthaeus, W. H., Goldstein, M. L., & Plante, D. 1988, J. Geophys. Res., 93, 14383
Bemporad, A. 2008, ApJ, 689, 572
Bemporad, A., Poletto, G., Suess, S. T., Ko, Y.-K., Schwadron, N. A., Elliott, H. A., & Raymond, J. C. 2006, ApJ, 638, 1110
Bhattacharjee, A., & Yuan, Y. 1995, ApJ, 449, 739
Biernat, H. K., Heyn, M. F., & Semenov, V. S. 1987, J. Geophys. Res., 92, 3392
Biskamp, D. 1986, Phys. Fluids, 29, 1520
Biskamp, D. 1990, in NATO Advanced Research Workshop on Physical Processes in Hot Cosmic Plasmas, ed. W. Brinkmann, A. C. Fabian, & F. Giovannelli (Dordrecht: Kluwer), 255
Biskamp, D. 1993, Nonlinear Magnetohydrodynamics (Cambrigde Monographs on Plasma Physics) (New York: Cambridge Univ. Press)
Bobrova, N. A., & Syrovatskii, S. I. 1980, Sov. J. Plasma Phys., 6, 1
Bulanov, S. V., Syrovatskii, S. I., & Sakai, J. 1978, JETP Lett., 28, 177
Chen, P. F., Shibata, K., Brooks, D. H., & Isobe, H. 2004, ApJ, 602, L61
Ciaravella, A., & Raymond, J. C. 2008, ApJ, 686, 1372
Ciaravella, A., Raymond, J. C., Li, J., Reiaer, P., Gardner, L. D., Ko, Y.-K., & Fineschi, S. 2002, ApJ, 575, 1116
Drake, J. F., Swisdak, M., Schoeffler, K. M., Rogers, B. N., & Kobayashi, S. 2006, Geophys. Res. Lett., 33, L13105
Dungey, J. W. 1958, Cosmic Electrodynamics (New York: Cambridge Univ. Press), 98
Forbes, T. G., & Acton, L. W. 1996, ApJ, 459, 330
Forbes, T. G., & Malherbe, J. M. 1991, Solar Phys., 135, 361
Forbes, T. G., & Lin, J. 2000, J. Atmos. Sol.-Terr. Phys., 62, 1499
Furth, H. P., Killeen, J., & Rosenbluth, M. N. 1963, Phys. Fluids, 6, 459
Gosling, J. T. 2007, ApJ, 671, L73
Ko, Y., Raymond, J. C., Lin, J., Lawrence, G., Li, J., & Fludra, A. 2003, ApJ, 594, 1068
Lazarian, A., & Vishniac, E. T. 1999, ApJ, 517, 700
Li, J., Jewitt, D. C., & LaBonte, B. J. 2000, ApJ, 539, L67
Lin, J. 2002, Chin. J. Astron. Astrophys., 2, 539
Lin, J., & Forbes, T. G. 2000, J. Geophys. Res., 105, 2375
Lin, J., Ko, Y.-K., Sui, L., Raymond, J. C., Stenborg, G. A., Jiang, Y., Zhao, S., & Mancuso, S. 2005, ApJ, 622, 1251
Lin, J., Li, J., Forbes, T. G., Ko, Y.-K., Raymond, J. C., & Vourlidas, A. 2007, ApJ, 658, L123
Litvinenko, Y. 1996, ApJ, 462, 997
Loureiro, N. F., Schekochihin, A. A., & Cowley, S. C. 2007, Phys. Plasma, 14, 100703
Miller, J. A., Cargill, P. J., & Emslie, A. G. 1997, JGR, 102, 14631
Noci, G., Kohl, J. L., & Withbroe, G. L. 1987, ApJ, 315, 706
Onofri, M., Isliker, H., & Vlahos, L. 2006, Phys. Rev. Lett., 96, 151102
Petschek, H. E. 1964, in Proc. AAS–NASA Symp., Physics of Solar Flares, ed. W. N. Hess (Washington, DC: NASA Sci. Tech. Inform. Div.), 425
Priest, E. R. 1982, Solar Magnetohydrodynamics (Boston, MA: Reidel), 127
Priest, E. R. 1985, Rep. Prog. Phys., 48, 955
Priest, E. R., & Forbes, T. 2000, Magnetic Reconnection—Magnetohydrodynamics Theory and Applications (New York: Cambridge Univ. Press)
Pritchett, P. L., Lee, Y. C., & Drake, J. F. 1980, Phys. Fluids, 23, 1368
Pudovkin, M. I., & Semenov, V. S. 1985, Space Sci. Rev., 41, 1
Rechester, A. B., & Stix, T. H. 1976, Phys. Rev. Lett., 36, 587
Rijnbeek, R. P., Biernat, H. K., Heyn, M. F., Semenov, V. S., & Farrugia, C. J. 1989, Ann. Geophys., 7, 297
Riley, P., Lionello, R., Mikić, Z., Linker, J. A., Clark, E., Lin, J., & Ko, Y.-k. 2007, ApJ, 655, 591
Semenov, V. S., Heyn, M. F., & Kubyshkin, I. V. 1983a, Sov. Astron., 27, 660
Semenov, V. S., Kubyshkin, I. V., Heyn, M. F., & Biernat, H. K. 1983b, J. Plasma Phys., 30, 321
Semenov, V. S., Vasilyev, E. P., & Pudovkin, A. I. 1984, Geomagn. Aeron., 24, 370
Stix, T. H. 1976, Phys. Rev. Lett., 36, 521

Strauss, H. R. 1986, Phys. Fluid, 29, 3668
Strauss, H. R. 1988, ApJ, 326, 412
Tajima, K., & Shibata, K. 2002, Plasma Astrophysics (Cambridge, MA: Persus)
van Ballegooijen, A. A., & Cranmer, S. R. 2008, ApJ, 682, 644
Vršnak, B., & Skender, M. 2005, Sol. Phys., 226, 97
Webb, D. F., Burkepile, J., Forbes, T. G., & Riley, P. 2003, J. Geophys. Res., 108, 1440
Wood, P., & Neukirch, T. 2005, Solar Phys., 226, 73
Yokoyama, T., Akita, K., Morimoto, T., Inoue, K., & Newmark, J. 2001, ApJ, 546, L69